

# Synthesis and Characterization of Folate Conjugated Boron Nitride Nanocarriers for Targeted Drug Delivery

Elizaveta S. Permyakova,<sup>\*,†,ID</sup> Irina V. Sukhorukova,<sup>†,ID</sup> Liubov Yu. Antipina,<sup>†,‡</sup> Anton S. Konopatsky,<sup>†</sup> Andrey M. Kovalskii,<sup>†</sup> Andrei T. Matveev,<sup>†</sup> Oleg I. Lebedev,<sup>§</sup> Dmitri V. Golberg,<sup>||,⊥</sup> Anton M. Manakhov,<sup>†</sup> and Dmitry V. Shtansky<sup>\*,†,ID</sup>

<sup>†</sup>National University of Science and Technology “MISIS”, Leninsky prospect 4, Moscow 119049, Russia

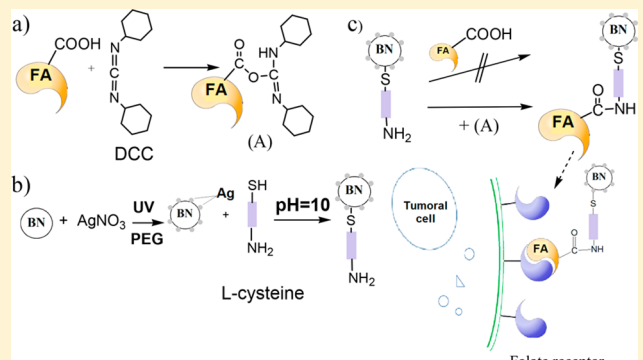
<sup>‡</sup>Institute of Biochemical Physics RAS, 4 Kosygin str., Moscow 119334, Russia

<sup>§</sup>Laboratoire CRISMAT, UMR 6508, CNRS-ENSICAEN, 6Bd Marechal Juin, 14050 Caen, France

<sup>||</sup>National Institute for Materials Science (NIMS), Namiki 1-1, Tsukuba, Ibaraki 3050044, Japan

<sup>⊥</sup>Queensland University of Technology (QUT), Second George St., Brisbane, QLD 4000, Australia

**ABSTRACT:** We have developed advanced folate bonded to boron nitride (BN) nanocarriers with a high potential for targeted drug delivery. The folic acid (FA) molecules were successfully conjugated to BN nanoparticles (BNNPs) in three consecutive stages: (i) FA preactivation by *N,N'*-dicyclohexylcarbodiimide (DCC), (ii) BNNP modification by AgNPs and their further NH<sub>2</sub>-functionalization with L-cysteine, and (iii) final conjugation of activated FA to modified BNNPs. To shed light on the FA-BNNPs binding mechanism, detailed energetic analysis of the atomic structure and stability of the FA-BNNPs system using density functional theory (DFT) calculations was carried out. The results indicated that the FA was successfully bonded with the BNNPs by a condensation reaction between amino groups of Cyst-Ag/BNNPs and carboxyl groups of FA using DCC. Theoretical analysis also demonstrated that the grafting of FA to the surface of BNNP does not affect FA targeting properties.



## 1. INTRODUCTION

Cancer is one of the leading causes of mortality worldwide. According to the world health organization, cancer was responsible for 8.8 million deaths in 2015, i.e., approximately every sixth death is caused by cancer. The traditional therapeutic approaches in a cancer treatment include chemotherapy, radiation, and surgery. However, every year more and more attention is given to a delivery of drug molecules into living cells.<sup>1</sup> Therefore, new drug delivery systems for cancer therapy and diagnosis are being actively developed. Inorganic nanomaterials, such as nanoparticles (NPs), nanotubes, and nanowires, exhibit advanced physicochemical properties promising for various biological applications,<sup>2–5</sup> including their utilization as new molecular transporters. To effectively treat complex malignant tumors, multifunctional nanomedicine with targeting and imaging properties, as well as controlled drug release should be designed and exploited. The redox-responsive nanocontainers, which can sense the differences in redox status and release the incorporated therapeutic agent in response to the intracellular reductive environment, allow one to achieve a significant therapeutic action with minimal side effects. Although redox-sensitive nanocarriers can be designed from both organic and inorganic materials, recent drug delivery systems are mostly based on inorganic nanomaterials due to the simplicity of their synthesis

and modification, as well as their attractive physicochemical characteristics.<sup>6–8</sup>

Boron nitride NPs (BNNPs) can be utilized as effective drug-delivery nanocarriers due to their nontoxicity for living cells and highly developed surface that can be effectively saturated with drug. The modification of the BNNP surface by different ligands makes them a specific drug delivery agent for the therapy of tumor diseases. It has been reported<sup>9,10</sup> that the metabolism of cancer cells requires a large amount of folic acid (FA) and cancer cells overexpress the folate receptors (FRs),<sup>11</sup> which has a high affinity toward FA.<sup>12</sup> Folic acid or its conjugates reversibly bind with the FRs, which are abundantly present on the cancer cell surface and easily penetrate through cellular membrane by receptor mediated endocytosis.<sup>13,14</sup> Recently, it has been reported that FA successfully forms conjugates with quantum dots,<sup>15</sup> iron oxide NPs,<sup>16</sup> gold NPs,<sup>21</sup> and others. Such conjugates have been widely used in cancer cell targeting, tumor imaging, and drug delivery.<sup>6–8,12–17,19–33</sup>

Folic acid has a complex aromatic structure and various types of free functional groups (carboxyl-, amino-, and hydroxyl

Received: November 2, 2017

Revised: November 20, 2017

Published: November 22, 2017

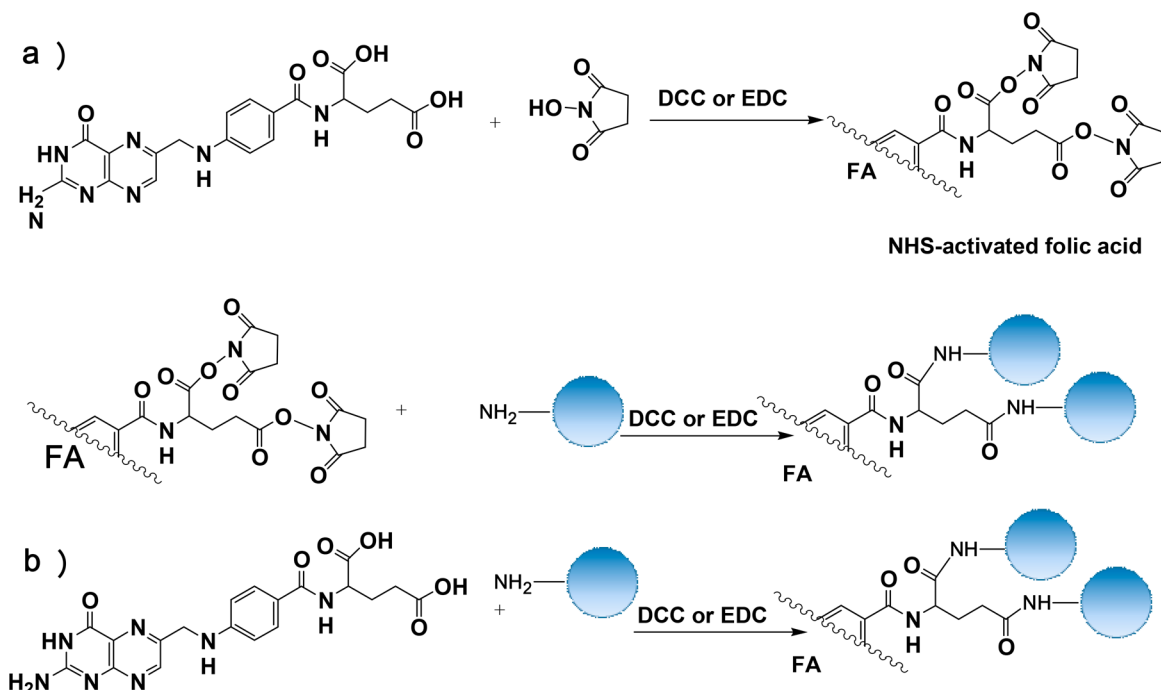


**Figure 1.** Synthesis scheme of folate-conjugated drug delivery system (DDS) using carbodiimides: (a) activation of carboxyl groups by *N*-hydroxysuccinimide (NHS) and carbodiimide; (b) activation of carboxyl groups by carbodiimide.

groups), but typically the FA is immobilized via a carboxyl group. The investigation of interaction between FA and folate binding protein (FBP), the soluble form of the cellular membrane-bound FR, demonstrated that covalent binding through carboxyl groups did not lead to a decrease in affinity of FBP to FA. However, when the FA is immobilized via hydroxyl or amino groups that are located in the active binding center, the affinity of FA to FBP is decreasing.<sup>18</sup>

Figure 1 shows a scheme of folate conjugate synthesis using carbodiimides. Carbodiimide compounds, being zero-length cross-linkers, provide the most robust and versatile method for direct conjugation of carboxylate to amines via amide linkage.<sup>19–21</sup> The most commonly used carbodiimides are the water-soluble 1-ethyl-3-(3-(dimethylamino)propyl)carbodiimide for aqueous cross-linking and the water-insoluble *N,N'*-dicyclohexylcarbodiimide (DCC) for nonaqueous organic synthesis. In some cases, after preliminary activation of the carboxyl groups by *N*-hydroxysuccinimide esters the reaction with amino groups can occur (Figure 1).<sup>22–28</sup>

To immobilize the FA molecules onto the NP surface using amide linkage, its surface must be functionalized with amine groups. For example, cross-linking of amine groups with gold NPs was achieved using thiol–gold chemistry. The strong S–Au bond (ca. 50 kcal mol<sup>−1</sup>)<sup>29</sup> allowed for simple anchoring of different chemical species to the surface of gold NPs, regardless of their molecular sizes. The commonly used cross-linking reagents containing amines and thiol groups are 4-aminothiophenol<sup>20</sup> and cysteine.<sup>30</sup>

Nanoparticles, regardless of their nature, can be also functionalized by coating their surface with a polymer layer containing amine groups, for example PEG-NH<sub>2</sub>,<sup>31</sup> PLGA-*b*-PEG-NH<sub>2</sub>,<sup>27</sup> PEI-NH<sub>2</sub>,<sup>32</sup> (3-aminopropyl)triethoxysilane (APTES -NH<sub>2</sub>),<sup>19,25</sup> and (3-aminopropyl)trimethoxysilane (APTMS-NH<sub>2</sub>).<sup>24</sup> Note, however, that in the case of porous NPs used as nanocarriers, APTES -NH<sub>2</sub>/APTMS-NH<sub>2</sub> are not suitable, because the NPs are covered by trimethoxy/ethoxysilane layer, hereby changing the NP morphology.

Another interesting approach is to use noncovalent attachment of FA to the NP surface. Rzayev et al.<sup>33</sup> described the synthesis of antibacterial polymer thin films containing silver cations. Intercalated nanocomposites, in which FA conjugated with octadecyl amine-montmorillonite (ODA-MMT) and Ag-montmorillonite (Ag-MMT) due to electrostatic interactions, formed multilayer composite.<sup>33</sup> The therapeutic effect demonstrated on L929 fibroblasts and DLD-1 cancer cells was achieved via interaction of amine groups with DNA-COOH sites and complexing of DNA with silver NPs under the formation of DNA-COOH…Ag complexes. The latter altered the DNA–protein and protein–protein interactions by destroying the self-assemble structural behaviors and cellular functions of DNA macromolecules.

In addition to the methods described above, there are a number of studies in which commercially available folate derivatives were used. For example, Cheng et al.<sup>34</sup> used a mercapto group-terminated poly(ethylene glycol)folic acid (SH-PEG-FA) and polydopamine to coat mesoporous silica NPs (MSNPs) to develop a versatile pH-responsive drug delivery system (DDS) for cancer therapy. First, doxorubicin(DOX)-loaded MSNPs were synthesized and then coated with polydopamine. Then, FA derivatives (FA-PEG-SH) were attached to the nanocomposites via Michael addition reaction to target specific cells with FA receptors. When MSNPs penetrate into cancer cells, low pH in cellular endosomes leads to the degradation of the pH-sensitive PDA coating, hereby releasing DOX to kill the cells. Note that the application of this approach requires the usage of rather expensive reagents.

Recently, we developed an original and simple method aimed at the fabrication of BNNPs with peculiar petal-like surfaces.<sup>35</sup> Thereafter we demonstrated that DOX-loaded BNNPs are promising nanocarriers for fighting tumor cells with multiple drug resistance (MDR).<sup>36</sup> In this work we are making an important follow-up step in developing advanced BNNP-based nanocarriers for targeted drug delivery to tumor cells. The FA molecules were conjugated to BNNPs modified with silver NPs

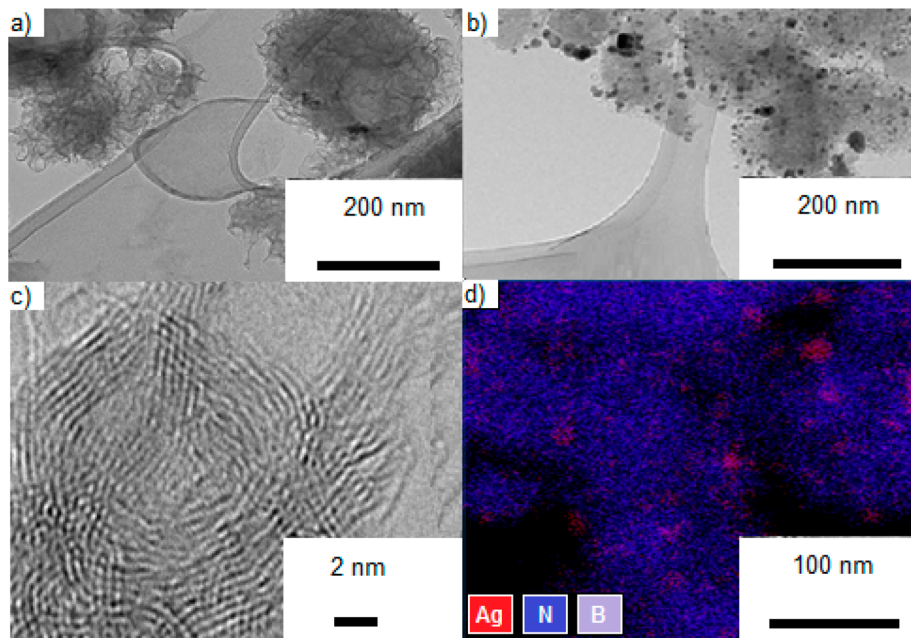


**Figure 2.** TEM images of BNNPs (a, c) before and (b) after AgNP deposition and (d) EDX spectroscopy mapping of Ag/BNNP nanohybrid.

(AgNPs) to provide coupling of FA to BNNPs. To shed a light on the FA-BNNPs binding mechanism, detailed energetic analysis using atomistic simulations was carried out.

## 2. EXPERIMENTAL SECTION

**2.1. Materials.** The following reagents were used: folic acid, L-cysteine (Cyst) (Panreac Applichem), N,N'-dicyclohexylcarbodiimide (DCC), silver nitrate (Alfa Aesar), dimethyl sulfoxide (DMSO), PEG (Prime Chemical Group), boron power (AVIABOR), ammonia solution, dichloromethane, and acetonitrile (Cupavna reactive).

**2.2. Preparation of Ag/BNNP Nanohybrids.** BNNPs were prepared through a chemical vapor deposition method as described elsewhere.<sup>36</sup> The BNNPs, 100–200 nm in size, had a petalled structure and consisted of a large number of BN nanosheets with a width of 30–40 nm and a length of 20–25 nm. Ag/BNNP nanohybrids were obtained as follows: 100 mg of BNNPs was dispersed in 50 mL of polyethylene glycol (PEG) by ultrasonic treatment on a Bandelin HD2200 unit mounted on a Wisestir MSH-20A magnetic stirrer at a 400 rpm for 3 min. After completion of the dispersion, 75 mg of silver nitrate ( $\text{AgNO}_3$ ) was added to the BNNPs/PEG suspension. Then the BNNPs/PEG/ $\text{AgNO}_3$  suspension was irradiated with the ultraviolet (UV) light using a UV lamp with a wavelength  $\lambda = 185$  nm for 30 min. During UV irradiation the BNNPs/PEG/ $\text{AgNO}_3$  suspension was also mixed using a magnetic stirrer. At the final stage, centrifugation on a Universal 320 centrifuge (Hettich) was performed three times in a row and then the resulting mixture was washed with distilled water. The as-synthesized Ag/BNNP nanohybrids were characterized using Fourier-transform infrared (FTIR) spectroscopy, X-ray photoelectron spectroscopy (XPS), and scanning electron microscopy (SEM).

**2.3. NH<sub>2</sub>-Functionalization of Ag/BNNPs.** NH<sub>2</sub>-functionalization of the Ag/BNNP surface was carried out according to the procedure described elsewhere.<sup>37</sup> A 40 mg amount of Ag/BNNPs was added into 40 mL of bidistilled water ( $\text{H}_2\text{O}_{\text{mq}}$ ), and the mixture was dispersed for 15 min. The resulting suspension was adjusted to pH 10 by adding 60  $\mu\text{L}$  of an aqueous

ammonia solution ( $\text{NH}_3\text{-H}_2\text{O}$ ). Then, 5 mL of an aqueous solution of Cyst ( $10^{-3}$  M) was added to the reaction mixture and stirred at room temperature for 24 h. Finally, the particles were washed three times with distilled water and dried. The NH<sub>2</sub>-functionalized Ag/BNNPs were characterized by FTIR spectroscopy and XPS analysis.

**2.4. Conjugation of FA to Ag/BNNPs.** Ten milligrams of FA was dissolved in 10 mL of dimethyl sulfoxide (DMSO), then 2 mg of DCC was added. The mixture was added to a pre-dispersed solution of Cyst-Ag/BNNPs in 10 mL of methylene chloride ( $\text{CH}_2\text{Cl}_2$ ). The reaction mixture was stirred for 24 h at room temperature. After completion of the chemical reaction, the Ag/BNNPs were rinsed with distilled water and finally dried. The FA-conjugated Ag/BNNPs were characterized by IR spectroscopy, XPS, and Fourier transform ion cyclotron resonance mass spectrometry (FT ICR MS).

**2.5. Material Characterization.** The morphology of synthesized BNNPs and Ag/BNNPs nanohybrids was studied using a scanning electron microscope JSM-7600F (JEOL) equipped with the energy-dispersive X-ray (EDX) detector. Transmission electron microscopy (TEM), including high resolution TEM (HRTEM) imaging and selected-area electron diffraction (SAED), was carried out using a Tecnai G2 30 UT microscope operated at 300 kV and having 0.17 nm spatial resolution. Chemical and phase compositions were analyzed by EDX spectroscopy using a 80 mm<sup>2</sup> X-Max EDX detector (Oxford Instruments) and FTIR spectroscopy with a Vertex 70v vacuum spectrometer (Bruker) in a range of 400–4000 cm<sup>-1</sup> using the partial internal reflection device. XPS studies of the BNNPs, Ag/BNNPs, Cyst-Ag/BNNPs, and FA-Cyst-Ag/BNNPs samples were carried out on an Axis Ultra DLD instrument (Kratos Analytical Ltd.) equipped with a monochromatic Al K $\alpha$  X-ray source ( $h\nu = 1486.6$  eV). To reveal the structure of the FA-Cyst-Ag/BNNPs nanohybrids in more detail, they were added into the mixture of water-acetonitrile (50/50) with 0.1% formic acid. Then the sample was centrifuged and the supernatant was selected. The sample was analyzed by FT ICR MS using an Apex Ultra unit (Bruker) with electrospray ionization at ionizing potential on a capillary of 4 kV.

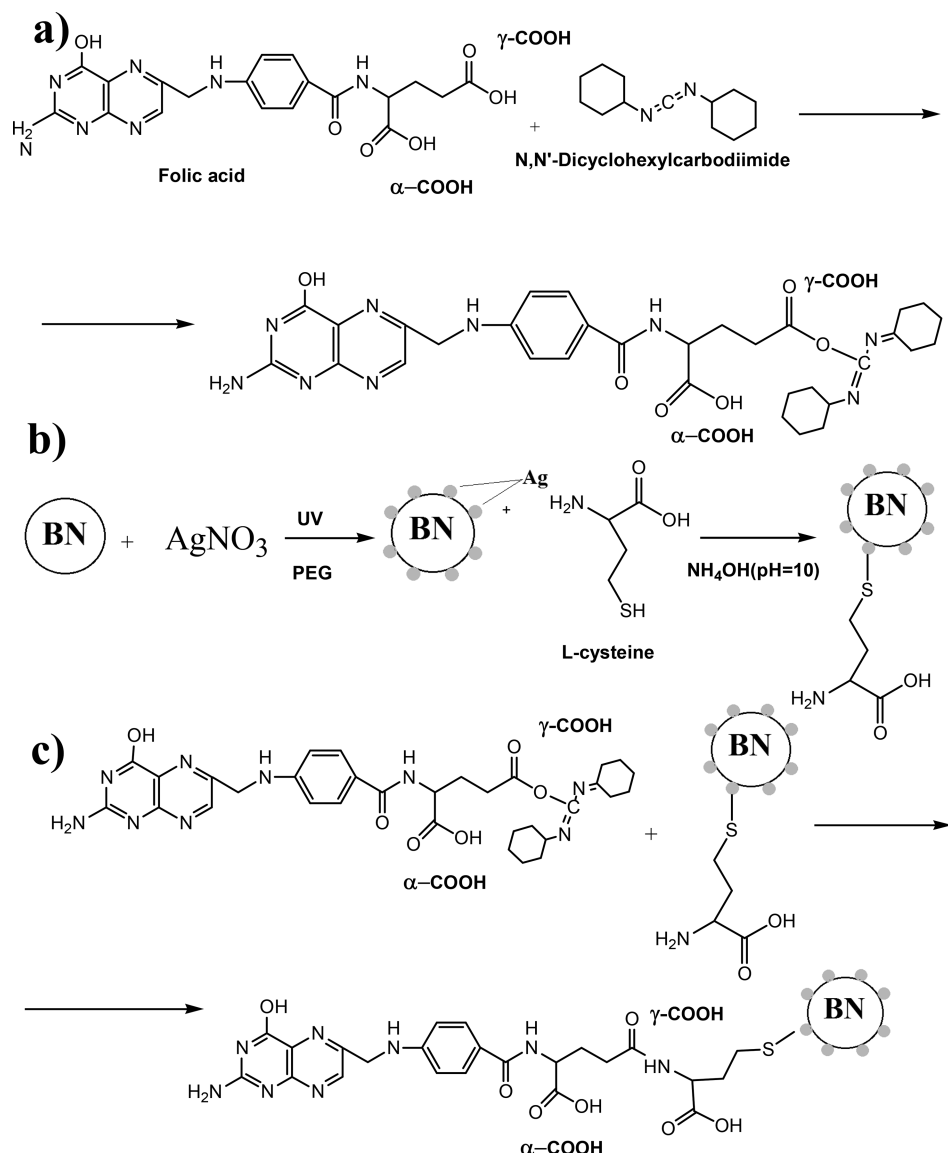


Figure 3. Schematics of activation of FA (a), modification of BNNPs (b), and final fabrication of FA-Cyst-Ag/BNNP complexes (c).

The rate of solution supply to electrospray was kept constant at  $2 \mu\text{L}/\text{min}$  and the measuring range was  $100$ – $1000 \text{ m/z}$ .

**2.6. Atomistic Simulations.** *Ab initio* calculations of the atomic structure and stability of the FA-BNNPs system were performed using density functional theory (DFT)<sup>38,39</sup> within the generalized gradient approximation (GGA) using the normalized Troullier–Martins pseudopotentials<sup>40</sup> in the SIESTA software package.<sup>41–43</sup> Numerical pseudoatomic wave functions were used as a basis for atomic localized orbitals. The system was modeled as a supercell with the sufficiently large vacuum gap ( $\geq 15 \text{ \AA}$ ) to exclude the intermolecular interaction in the nonperiodic direction. The structural relaxation was performed until the forces acting on each atom became less than  $0.03 \text{ eV/\AA}$ . The plane-wave energy cutoff was set to  $175 \text{ Ry}$ . To calculate the equilibrium atomic structures, the Brillouin zone was sampled according to the Monkhorst–Pack scheme,<sup>44</sup> and the  $k$ -grid cutoff was equal to  $6 \text{ \AA}$ . For calculation of electronic properties, the  $k$ -grid cutoff was equal to  $24 \text{ \AA}$ . The accuracy of the calculation was confirmed by the geometric parameters of the system. In particular, for *h*-BN, the lattice parameter  $a$  obtained in our calculations was  $2.51 \text{ \AA}$  and the distance between the layers

was  $3.63 \text{ \AA}$ , whereas the experimental data for *h*-BN give the values of  $2.50$  and  $3.33 \text{ \AA}$ ,<sup>45</sup> respectively.

### 3. RESULTS AND DISCUSSION

**3.1. Preparation and Characterization of FA-Cyst-Ag/BNNPs Nanohybrids.** Microstructures of BNNPs just before and after the deposition of AgNPs are illustrated in Figure 2. It can be seen that BNNPs,  $150$ – $300 \text{ nm}$  in size, have a spherical shape and their surface is formed by numerous *h*-BN petals (Figure 2a,c). Spherical AgNPs,  $5$ – $40 \text{ nm}$  in diameter, densely populate the surface of BNNPs (Figure 2b). The EDS mapping, presented in Figure 2d, further confirms that the AgNPs are uniformly distributed over the BNNP surface. From TEM images it can be also seen that the precipitation of AgNPs on the BNNP surface does not lead to a noticeable change in their morphology.

The three main stages of FA-Cyst-Ag/BNNP nano hybrid fabrication: (i) FA activation, (ii) BNNP modification, and (iii) conjugation of activated FA to modified BNNPs, as well as the chemical structures of the modified Ag/BNNPs conjugates are depicted in Figure 3. Carboxyl-groups of FA were preactivated by DCC (Figure 3a). The cysteine forms coordinate

bonds in which a pair of cystine electrons ( $R-S^-$ , Lewis base) were donated to the  $Ag^+$  (Lewis acid), leading to the formation of a zero oxidation state of Ag atoms ( $Ag^0$ ) that were chemically bonded to the hydrocarbon chains of the cysteine via the Ag–S bonds (Figure 3b).<sup>46</sup> During the final stage, FA was grafted to the surface of BNNPs under a condensation reaction between amino groups of Cyst-Ag/BNNPs and carboxyl groups of FA using DCC (Figure 3c).

Figure 4 compares the FTIR spectra of the Ag/BNNPs, Cyst-Ag/BNNPs, and FA-Cyst-Ag/BNNPs nanohybrids. The Ag/BNNPs

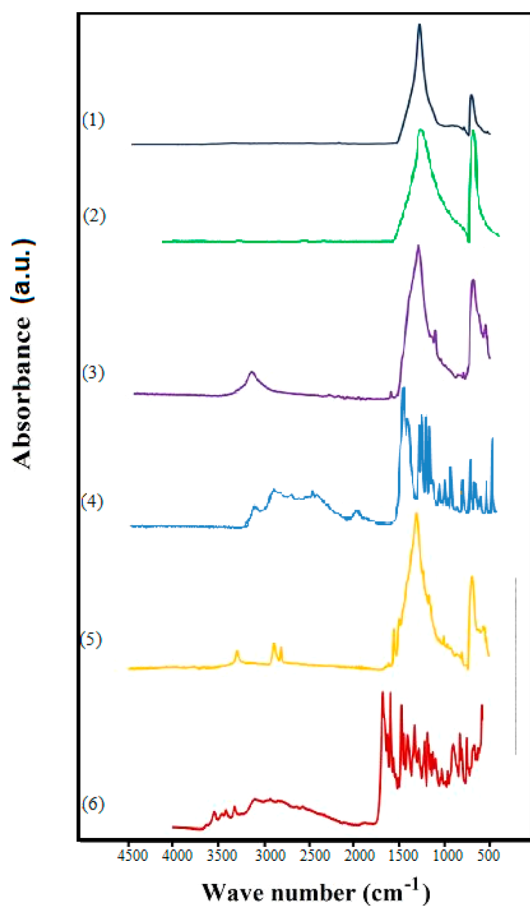


**Figure 4.** FTIR spectra of (1) Ag/BNNPs, (2) BNNPs, (3) Cyst-Ag/BNNPs, (4) L-cysteine, (5) FA-Cyst-Ag/BNNPs, and (6) FA.

sample has a strong asymmetric band at around  $1359\text{ cm}^{-1}$ , corresponding to the B–N stretching vibration, and a less intense band at  $769\text{ cm}^{-1}$ , which is ascribed to the B–N–B bending vibration.<sup>47</sup> Moreover, the FTIR spectrum of the Ag/BNNPs has a region with a high absorbance between  $400$  and  $720\text{ cm}^{-1}$ .<sup>34</sup> The presence of AgNPs does not affect the shape and positions of the peaks on the BNNP spectrum because Ag absorbs at  $420\text{ cm}^{-1}$  and, therefore, makes an insignificant contribution to the BN peaks. The strong and sharp peaks observed at  $2916$  and  $2845\text{ cm}^{-1}$  in the FTIR spectrum of FA-Cyst-Ag/BNNPs

correspond to the asymmetric and symmetric stretching of methylene groups, respectively. An additional peak located at  $3400\text{ cm}^{-1}$  corresponds to the amino groups in the Cyst-Ag/BNNPs and FA-Cyst-Ag/BNNPs samples. The distinct peak at  $1700\text{ cm}^{-1}$  in the spectrum of FA-Cyst-Ag/BNNPs complexes was assigned to the C=O amide stretching of FA molecule.

The Ag/BNNPs, Cyst-Ag/BNNPs, and FA-Cyst-Ag/BNNPs nanohybrids were then analyzed by XPS to obtain quantitative information regarding the elemental composition and surface chemical environments. High-resolution XPS B 1s, N 1s, and C 1s spectra are shown in Figure 5. The XPS B 1s spectrum of the Ag/BNNPs, Cyst-Ag/BNNPs, and FA-Cyst-Ag/BNNPs samples was deconvoluted into two peaks located at  $190.6$  and  $192\text{ eV}$  corresponding to the  $B-N$  and  $B_2O_3$ , respectively (Figure 5a). The single maximum observed in the XPS N 1s spectrum of the Ag/BNNPs can be well divided into two main components located at  $398.1$  and  $399.1\text{ eV}$ ; these are attributed to the  $B-N$  and  $C-N$ , respectively (Figure 5b). In the XPS N 1s spectra of the Cyst-Ag/BNNPs and FA-Cyst-Ag/BNNPs samples, as a result of peak decomposition additional small feature appears at  $400.4\text{ eV}$  due to the amides  $N-C=O$  coming from FA. Thus, the XPS results clearly indicate that the FA molecules are chemically bonded through amide linkage to the surface of Cyst-Ag/BNNPs. The high-resolution XPS C 1s spectra of the Cyst-Ag/BNNPs and FA-Cyst-Ag/BNNPs samples (Figure 5c) were deconvoluted into four peaks positioned at  $285.0$ ,  $286.4$ ,  $288.5$ , and  $290.0\text{ eV}$ , which could be attributed to the  $\underline{CH}_x$ ,  $-NH-C/C-O$ ,  $-C=O/N-C=O$  and  $-C(O)O$  groups, respectively.

Table 1 summarizes the results of quantitative XPS analysis. The N/B ratio is an important parameter to quantitatively analyze the grafting of Cyst and FA to the surface of BNNPs. As a first approximation, we can assume that the amount of nitrogen in the BNNPs is equal to  $0.77$ , as it was calculated from the corresponding XPS spectra of the Ag/BNNPs (Table 1).

The observed increase in the N/B ratio to  $0.9$  after BNNP surface fictionalization, and further to  $1.07$  after FA cross-linkage can be attributed to grafting respective molecules: cysteine (Cyst-Ag/BNNPs) and FA (FA-Cyst-Ag/BNNPs). Thus, the increment in N/B ratio at each modification stage can be calculated on the basis of an estimate of nitrogen contribution from Cyst and FA according to the following equations.

$$\Delta N_{\text{Cyst-Ag/BNNPs}} = \left[ \frac{N_{\text{Cyst-Ag/BNNPs}}}{B_{\text{Cyst-Ag/BNNPs}}} - \frac{N_{\text{Ag/BNNPs}}}{B_{\text{Ag/BNNPs}}} \right] \times [B]_{\text{Cyst-Ag/BNNPs}}$$

$$\Delta N_{\text{FA-Cyst-Ag/BNNPs}} = \left[ \frac{N_{\text{FA-Cyst-Ag/BNNPs}}}{B_{\text{FA-Cyst-Ag/BNNPs}}} - \frac{N_{\text{Cyst-Ag/BNNPs}}}{B_{\text{Cyst-Ag/BNNPs}}} \right] \times [B]_{\text{FA-Cyst-Ag/BNNPs}}$$

**Table 1.** Results of XPS Analysis

| sample           | concentration, at. % |      |      |      |     |     |     | N/B  | $\Delta N$ |
|------------------|----------------------|------|------|------|-----|-----|-----|------|------------|
|                  | O                    | C    | N    | B    | Na  | Ag  | S   |      |            |
| Ag/BNNPs         | 13.9                 | 51.0 | 15.3 | 19.8 |     | 0.1 |     | 0.77 |            |
| Cyst-Ag/BNNPs    | 10.2                 | 34.5 | 25.9 | 28.7 | 0.2 | 0.1 | 0.4 | 0.90 | 3.7        |
| FA-Cyst-Ag/BNNPs | 14.3                 | 47.9 | 19.5 | 18.3 |     | 0.1 |     | 1.07 | 3.1        |

Knowing the  $\Delta N$  value, we can calculate the concentration of atoms in FA molecule grafted to the Ag/BNNP nanoparticle. Given that the FA has a chemical formula  $C_{19}H_{19}N_7O_6$  and hydrogen is not detected by XPS, we can estimate the total atomic concentration of C, O, and N atoms (hereafter denoted as  $C_{FA}$ ). To calculate the  $C_{FA}$  values, we divided the  $\Delta N$  by 7

(number of N atoms in one FA molecule) and multiply it by the total number of C, O, and N atoms in one FA molecule:  $C_{FA} = \Delta N / 7 \times (19 + 7 + 6) = 14.2$  at. %. Then we should take into account that the results of quantitative analysis of XPS spectra are affected by additional C 1s and O 1s signals coming from the BNNP contaminations and carbon tape supporting the BNNPs

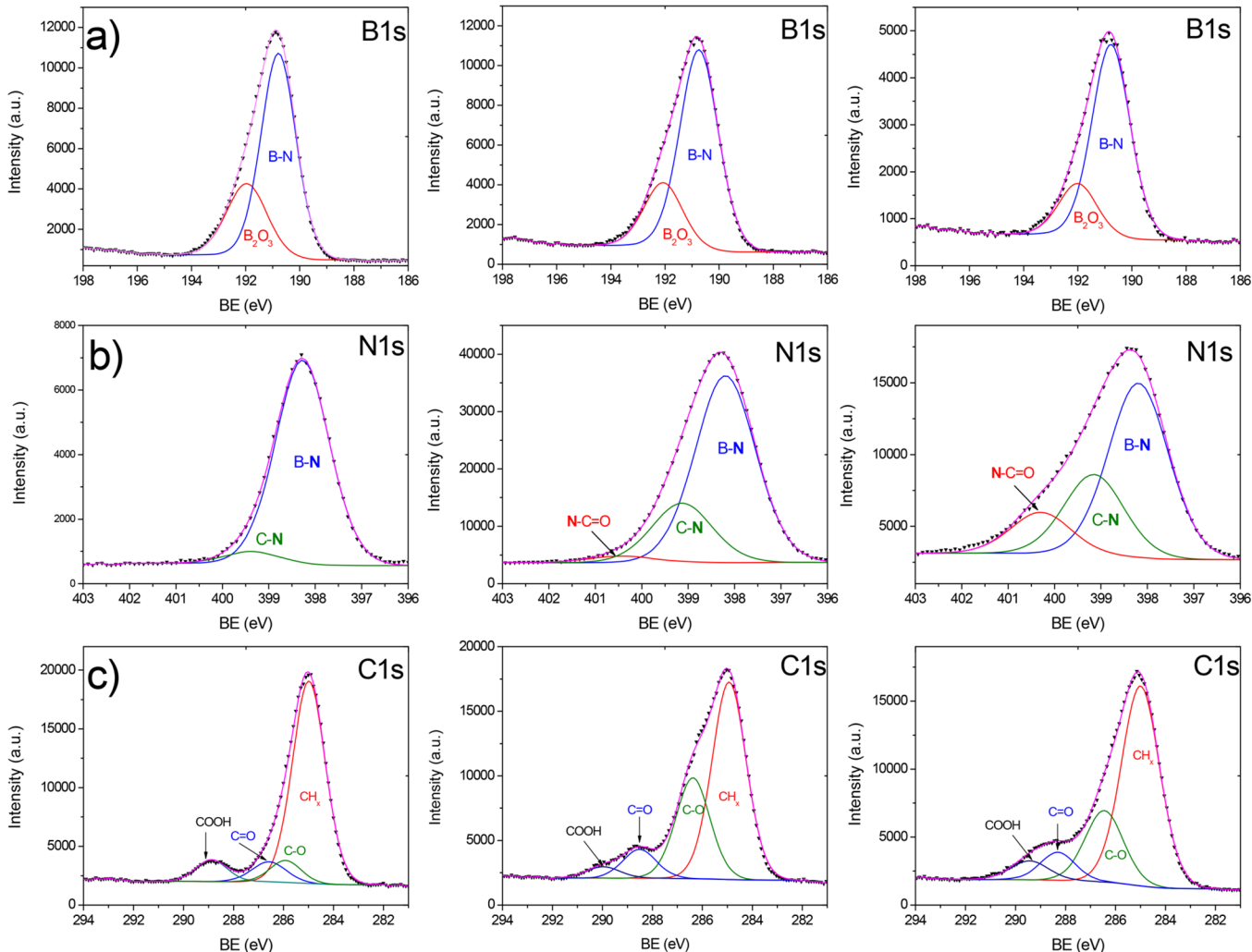


**Figure 5.** High-resolution XPS B 1s (a), N 1s (b), and C 1s (c) spectra of Ag/BNNPs (left column), Cyst-Ag/BNNPs (middle column), and FA-Cyst-Ag/BNNPs samples (right column).

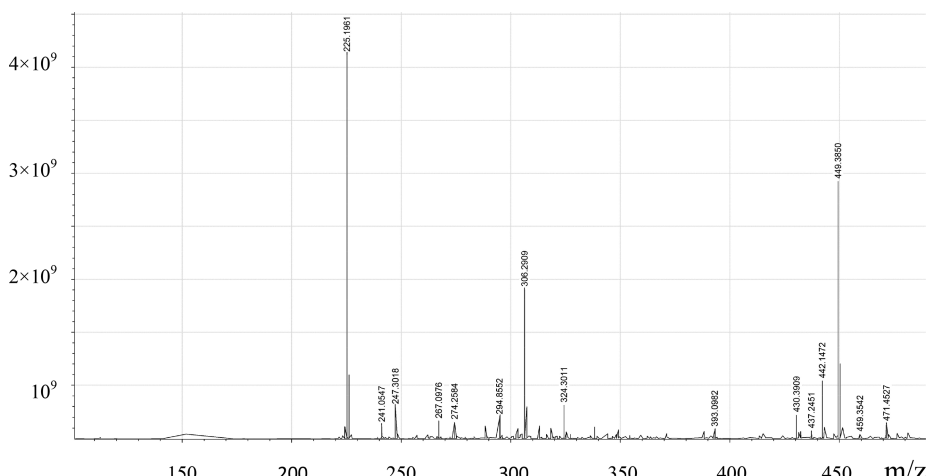


**Figure 6.** FT ICR MS spectrum of the FA-Cyst-Ag/BNNPs sample after the treatment with FA.

Table 2. Main Ions Detected by FT ICR MS

| compound                      | molecular formula   | ion type                              | <i>m/z</i> theoretical | <i>m/z</i> experimental |
|-------------------------------|---|---------------------------------------|------------------------|-------------------------|
| <i>N,N'</i> -dicyclohexylurea | C <sub>13</sub> H <sub>24</sub> N <sub>2</sub> O                | [M <sub>2</sub> + H] <sup>+</sup>     | 449.385                | 449.385                 |
| folic acid                    | C <sub>19</sub> H <sub>19</sub> N <sub>7</sub> O <sub>6</sub>   | [M + H] <sup>+</sup>                  | 442.138                | 442.138                 |
| <i>N,N'</i> -dicyclohexylurea | C <sub>13</sub> H <sub>24</sub> N <sub>2</sub> O                | [M + H] <sup>+</sup>                  | 225.196                | 225.196                 |
| PEG                           | [C <sub>2</sub> H <sub>4</sub> O] <sub>n</sub> H <sub>2</sub> O | [A <sub>8</sub> B + Na] <sup>+</sup>  | 393.210                | 393.210                 |
| PEG                           | [C <sub>2</sub> H <sub>4</sub> O] <sub>n</sub> H <sub>2</sub> O | [A <sub>9</sub> B + Na] <sup>+</sup>  | 437.245                | 437.245                 |
| PEG                           | [C <sub>2</sub> H <sub>4</sub> O] <sub>n</sub> H <sub>2</sub> O | [A <sub>10</sub> B + Na] <sup>+</sup> | 459.352                | 459.354                 |

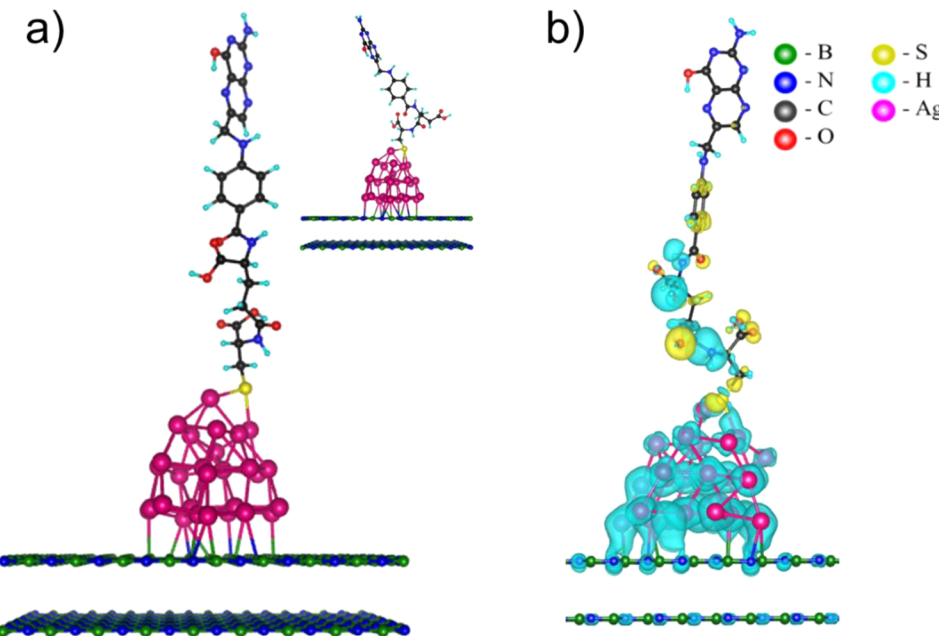


**Figure 7.** (a) Schematics of FA-Cyst-Ag/BNNPs ( $\gamma$ -COOH) with another possible but energy unfavorable type of bonding between Cyst-Ag/BNNPs and carboxyl groups of FA ( $\alpha$ -COOH) (inset). (b) Distribution of spatial charge density difference between FA-Cyst-Ag/BNNPs ( $\alpha$ -COOH) and corresponding freestanding parts. The loss and gain of charge are denoted by yellowish and bluish colors, respectively. The boron, nitrogen, carbon, oxygen, sulfur, hydrogen, and silver atoms are marked by green, blue, gray, red, cyan, and purple colors, respectively.

samples. Therefore, we normalized the obtained  $C_{FA}$  value to the concentration of BN, i.e., the concentration of B and N atoms in BNNP. We assumed equal contents of B and N in BN (denoted as  $C_{BN}$ ) and the total number of B and N atoms was calculated using a formula:  $C_{BN} = 2[B] = 36.6$ . Now we can normalize the  $C_{FA}$  concentration to the total amount of BN using the following equation:  $C_{FA}/C_{BN} = 14.2/36.6 = 0.39$ . The results indicate that approximately 39% of the BN surface is covered by FA molecules.

The structure of FA-Cyst-Ag/BNNPs conjugates was further analyzed by a FT ICR MS method. Although the method is very sensitive to the determination of different ion types, it has some weight limitations of samples for their ionization. In our case, organic molecules were covalently attached to the surface of Ag/BNNPs, 180–200 nm in diameter, which are too heavy for analyzing by FT ICR MS. Thus, the FA-Cyst-Ag/BNNPs sample was treated with formic acid to cleave the peptide bonds in the conjugate structure and the decomposed products were analyzed by FT ICR MS. Figure 6a demonstrates the FT ICR MS spectrum of the treated FA-Cyst-Ag/BNNPs sample, whereas the list of main ions detected is given in Table 2. The peaks related to *N,N'*-dicyclohexylurea (side product) and FA were observed, hereby indicating that FA was conjugated to BNNP surface. In addition, FT ICR MS peaks corresponding to PEG, which participated in the synthesis of BNNPs, were detected. These results clearly indicated that FA had been covalently grafted with BNNPs.

**Table 3. BE for Each Reaction Step during the Fabrication of FA-Cyst-Ag/BNNPs Nanohybrids**

| reaction                      | type of carboxyl group of FA |                |
|-------------------------------|------------------------------|----------------|
|                               | $\alpha$ -COOH               | $\gamma$ -COOH |
| activation of FA by DCC (FA*) | -0.73                        | -1.15          |
| AgNP + BNNPs                  | -5.27                        | -5.27          |
| Cyst + Ag/BNNPs               | -3.42                        | -3.43          |
| FA* + Cyst-Ag/BNNPs           | -2.76                        | -2.74          |

### 3.2. Simulation of FA-Cyst-Ag/BNNPs Nanohybrids.

To shed a light on the nature of chemical binding between FA and BNNPs, detailed energetic analysis using atomistic simulations was performed using the following approximations. Considering a relatively large size and small curvature of BNNPs, in the simplified model they were considered as an infinite *h*-BN sheet. The absence of electron transfer between physically bonded neighbored *h*-BN layers allows us to consider only a few atomic planes.

The AgNP on the BNNP surface was simulated as a 1 nm sized nanoparticle. Our preliminary calculations using both smaller (0.5 nm in diameter) and infinitely large AgNP (infinite Ag<sub>(111)</sub> slab) show that the AgNP with the size of 1 nm and infinite Ag slab display similar binding energy (BE) values for all three types of Ag/BNNPs, Cyst-Ag/BNNPs, and FA-Cyst-Ag/BNNPs nanocomposites obtained at different stages of functionalization.

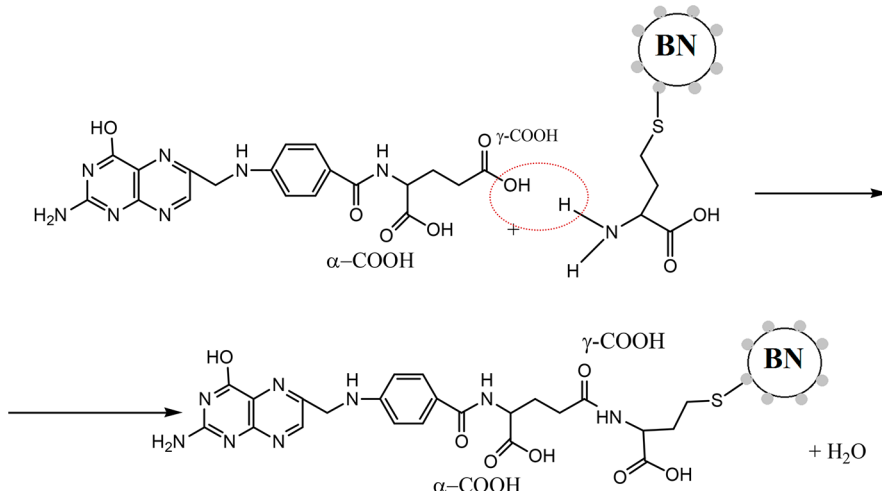


**Figure 8.** Schematics of nonactivated FA grafting to modified BNNP.

Thus, the results indicate that the AgNP of 1 nm in size can qualitatively describe the status of NPs on nanohybrids.

Then an Ag/BNNP nano hybrid was coupled with the Cyst amino acid (Figure 7a). According to the experimental data, in our theoretical model both virgin and activated (by 1,3-dicyclohexylcarbodiimide) FA were considered.

We calculated the BE  $E_b^n$  at each step of BNNP modification by FA as the difference between energy of system with adsorbed molecule ( $E_{\text{tot}}^n$ ) and the sum of total energies of the system in the previous step ( $E_{\text{tot}}^{n-1}$ ) and isolated molecule ( $E_m$ ):

$$E_b^n = E_{\text{tot}}^n - (E_{\text{tot}}^{n-1} + E_m)$$

The BE of various carboxyl groups at each BNNP modification step are summarized in Table 3. The addition of inactivated 1,3-dicyclohexylcarbodiimide FA to the Cyst-Ag/BNNPs system is thermodynamically unfavorable (the BE of such process is positive, i.e., 1.52 eV), whereas the activation of FA reduces the BE to a negative value of  $\sim -2.74$  eV. This result can be well explained by two factors: (i) water formation during FA activation stage (from the  $-H$  of the amino group of Cyst and  $-OH$  group of FA carboxyl group) (Figure 8) and (ii) the conversion of 1,3-dicyclohexylcarbodiimide to dicyclohexylurea through an intermediate step of O-acylated dicyclohexylurea formation (Figure 3a). This conversation lowers the total energy of the system due to the formation of additional bonds. This result agrees well with the experimental data.

We also considered the influence of the carboxyl group type in FA on the BE of FA with Cyst-Ag/BNNP hybrid. There are two carboxyl groups at the glutamic acid part of the FA, marked as  $\alpha$ - and  $\gamma$ -COOH groups in Figure 3a,b. The results indicate that there is practically no difference through which  $\alpha$ - or  $\gamma$ -COOH group end the activated FA is bonded ( $E_b = 2.76$  and 2.74 eV for  $\alpha$ -COOH and  $\gamma$ -COOH, respectively). However, there is a difference in the BE of DCC to FA ( $E_b = -0.73$  eV and  $-1.15$  eV for  $\alpha$ -COOH and  $\gamma$ -COOH, respectively). Therefore, although the grafting of FA to the Cyst-Ag/BNNP by different carboxyl groups is thermodynamically equivalent, the  $\gamma$ -COOH activation process should be simpler compared to  $\alpha$ -COOH (Figure 3).

For successful interaction of FA-modified BNNPs with folate receptors of cancer cells, it is important to keep the electronic structure of the pteroic acid end of FA unchanged. To understand the impact of Cyst-Ag/BNNP to the FA we calculated the

difference in spatially distributed electron density between the whole system and each separate part:

$$\rho_{\text{FA-Cyst-Ag/BNNPs}}^{\text{dis}} = \rho_{\text{FA-Cyst-Ag/BNNPs}}^{\text{total}} - \rho_{\text{FA}} - \rho_{\text{Cyst}} - \rho_{\text{Ag}} - \rho_{\text{BNNPs}}$$

The results of electron density calculations presented in Figure 7b indicate that the changes in the electron density of the resultant FA-Cyst-Ag/BNNPs nano hybrid can only occur in the region of FA-Cyst bonding, whereas the electronic structure of the pteroic acid end in FA will not change with respect to the pure, unbound molecule. Thus, the grafting of FA to the surface of BNNP should not affect FA targeting properties (Figure 8).

## 4. CONCLUSIONS

We have developed an advanced folate bonded to boron nitride nanocarriers with a high potential for targeted drug-delivery to tumor cells. The folic acid (FA) molecules were successfully conjugated to BN nanoparticles (BNNPs) modified with silver nanoparticles (AgNPs) to provide coupling of FA to BNNPs. This was achieved in three consecutive stages: (i) FA preactivation by  $N,N'$ -dicyclohexylcarbodiimide (DCC), (ii) BNNP modification by AgNPs and their further  $NH_2$ -functionalization with L-cysteine, and (iii) final conjugation of activated FA to modified BNNPs. *Ab initio* calculations indicated that preactivation of FA reduces the binding energy of various carboxyl groups at the BNNP surface. The FA was grafted to the surface of BNNPs by the condensation reaction between amino groups of Cyst-Ag/BNNPs and carboxyl groups of FA using DCC. The presence of FA in the FA-Cyst-Ag/BNNPs nano hybrid was documented by Fourier-transform infrared spectroscopy, X-ray photoelectron spectroscopy, and Fourier transform ion cyclotron resonance mass spectrometry. Theoretical analysis also indicated that the grafting of FA to the surface of BNNP had not affected FA targeting properties.

## ■ AUTHOR INFORMATION

### Corresponding Authors

\*E. S. Permyakova. E-mail: permyakova.elizaveta@gmail.com. Tel: +79162780199.

\*D. V. Shtansky. E-mail: shtansky@shs.misis.ru. Tel: +74992366629.

## ORCID®

Elizaveta S. Permyakova: 0000-0003-2581-0803

Irina V. Sukhorukova: 0000-0003-2458-164X

Dmitry V. Shtansky: 0000-0001-7304-2461

## Notes

The authors declare no competing financial interest.

## ACKNOWLEDGMENTS

The work was supported by the Ministry of Education and Science of the Russian Federation (Increase Competitiveness Program of NUST "MISiS" No. K2-2016-011) and Russian Foundation for Basic Research (16-08-00957). D.G. is grateful to the Australian Research Council for granting a Laureate Fellowship (FL160100089). L.Yu.A. acknowledges Grant of President of Russian Federation for government support of young PhD scientists (MK-3326.2017.2). The authors are grateful to the supercomputer cluster NUST "MISiS" kindly provided by Materials Modeling and Development Laboratory (supported via the Grant from the Ministry of Education and Science of the Russian Federation No. 14.Y26.31.0005) and to the Joint Supercomputer Center of the Russian Academy of Sciences.

## REFERENCES

- (1) Henry, C. M. New Drug Wrinkles in Drug Delivery. *Chem. Eng. News* **2004**, *82*, 37–42.
- (2) Alivisatos, P. The Use of Nanocrystals in Biological Detection. *Nat. Biotechnol.* **2004**, *22*, 47–52.
- (3) Kim, S.; Lim, Y. T.; Soltesz, E. G.; De Grand, A. M.; Lee, J.; Nakayama, A.; Parker, J. A.; Mihaljevic, T.; Laurence, R. G.; Dor, D. M.; et al. Near-Infrared Fluorescent Type II Quantum Dots for Sentinel Lymph Node Mapping. *Nat. Biotechnol.* **2004**, *22*, 93–97.
- (4) Taton, T. A.; Mirkin, C. A.; Letsinger, R. L. Scanometric DNA Array Detection with Nanoparticle Probes. *Science* **2000**, *289*, 1757–1760.
- (5) Cui, Y.; Wei, Q.; Park, H.; Lieber, C. M. Nanowire Nanosensors for Highly Sensitive and Selective Detection of Biological and Chemical Species. *Science* **2001**, *293*, 1289–1292.
- (6) Han, L.; Zhang, X. Y.; Wang, Y. L.; Li, X.; Yang, X. H.; Huang, M.; Hu, K.; Li, L. H.; Wei, Y. Redox-Responsive Theranostic Nanoplatforms Based on Inorganic Nanomaterials. *J. Controlled Release* **2017**, *259*, 40–52.
- (7) Bogdan, J.; Plawińska-Czarnak, J.; Zarzyńska, J. Nanoparticles of Titanium and Zinc Oxides as Novel Agents in Tumor Treatment: A Review. *Nanoscale Res. Lett.* **2017**, *12*, 225–240.
- (8) Chakravarty, R.; Goel, S.; Dash, A.; Cai, W. Radiolabeled Inorganic Nanoparticles for Positron Emission Tomography Imaging of Cancer: An Overview. *Q. J. Nucl. Med. Mol. Imaging* **2017**, *61*, 181–204.
- (9) Stea, B.; Backlund, P. S., Jr.; Berkey, P. B.; Cho, A. K.; Halpern, B. C.; Halpern, R. M.; Smith, R. A. Folate and Pterin Metabolism by Cancer Cells in Culture. *Cancer Res.* **1978**, *38*, 2378–2384.
- (10) Bertino, J. R. Cancer Research: from Folate Antagonism to Molecular Targets. *Best Pract. Res. Clin. Haematol.* **2009**, *22*, 577–582.
- (11) Gabizon, A.; Horowitz, A. T.; Goren, D.; Tzemach, D.; Mandelbaum-Shavit, F.; Qazen, M. M.; Zalipsky, S. Targeting Folate Receptor with Folate Linked to Extremities of Poly(Ethylene Glycol)-Grafted Liposomes: in Vitro Studies. *Bioconjugate Chem.* **1999**, *10*, 289–298.
- (12) Lu, Y.; Low, P. S. Folate-Mediated Delivery of Macromolecular Anticancer Therapeutic Agents. *Adv. Drug Delivery Rev.* **2012**, *64*, 342–352.
- (13) Grumezescu, A. M. *Nanobiomaterials in cancer therapy: Applications of nanobiomaterials*; Elsevier: Oxford, U.K., 2016.
- (14) Song, H.; Su, C.; Cui, W.; Zhu, B.; Liu, L.; Chen, Z.; Zhao, L. Folic Acid-Chitosan Conjugated Nanoparticles for Improving Tumor-Targeted Drug Delivery. *BioMed Res. Int.* **2013**, *2013*, 1–6.
- (15) Bwatanglang, I. B.; et al. In Vivo Tumor Targeting and Anti-Tumor Effects of 5-Fluorouracil Loaded, Folic Acid Targeted Quantum Dot System. *J. Colloid Interface Sci.* **2016**, *480*, 146–158.
- (16) Wang, X.; Tu, M.; Tian, B.; Yi, Y.; Wei, Z.; Wei, F. Synthesis of Tumor-Targeted Folate Conjugated Fluorescent Magnetic Albumin Nanoparticles for Enhanced Intracellular Dual-Modal Imaging into Human Brain Tumor Cells. *Anal. Biochem.* **2016**, *512*, 8–17.
- (17) Feng, S.; Zhang, H.; Yan, T.; Huang, D.; Zhi, C.; Nakanishi, H.; Gao, X.-D. Folate-Conjugated Boron Nitride Nanospheres for Targeted Delivery of Anticancer Drugs. *Int. J. Nanomed.* **2016**, *11*, 4573–4582.
- (18) Merzel, R. L.; Frey, C.; Chen, J.; Garn, R. Conjugation Dependent Interaction of Folic Acid with Folate Binding Protein. *Bioconjugate Chem.* **2017**, *28*, 2350–2360.
- (19) Hermanson, G. T. Zero-Length Crosslinkers. *Bioconjugate techniques*, third ed.; Elsevier: Oxford, U.K., 2013.
- (20) Liu, Q.; Xu, N.; Liu, L.; Li, J.; Zhang, Y.; Shen, C.; Shezad, K.; Zhang, L.; Zhu, J.; Tao, J. Dacarbazine-Loaded Hollow Mesoporous Silica Nanoparticles Grafted with Folic Acid for Enhancing Anti-Metastatic Melanoma Response. *ACS Appl. Mater. Interfaces* **2017**, *9*, 21673–21687.
- (21) Mansoori, G. A.; Brandenburg, K. S.; Shakeri-Zadeh, A. A Comparative Study of Two Folate-Conjugated Gold Nanoparticles for Cancer Nanotechnology Applications. *Cancers* **2010**, *2*, 1911–1928.
- (22) Aliboland, M.; Abnous, K.; Sadeghi, F.; Hosseinkhani, H.; Ramezani, M.; Hadizadeh, F. Folate Receptor-Targeted Multimodal Polymersomes for Delivery of Quantum Dots and Doxorubicin to Breast Adenocarcinoma: in Vitro and in Vivo Evaluation. *Int. J. Pharm.* **2016**, *500*, 162–178.
- (23) Su, X. A Graphene Quantum Dot@Fe<sub>3</sub>O<sub>4</sub>@SiO<sub>2</sub> Based Nanoprobe for Drug Delivery Sensing and Dual-Modal Fluorescence and MRI Imaging in Cancer Cells. *Biosens. Bioelectron.* **2017**, *92*, 489–495.
- (24) Kumar, P.; Tambe, P.; Paknikar, K. M.; Gajbhiye, V. Folate/N-Acetyl Glucosamine Conjugated Mesoporous Silica Nanoparticles for Targeting Breast Cancer Cells: A Comparative Study. *Colloids Surf., B* **2017**, *156*, 203–212.
- (25) Bharathiraja, S.; Santha Moorthy, M.; Manivasagan, P.; Seo, H.; Lee, K. D.; Oh, J. Chlorin E6 Conjugated Silica Nanoparticles for Targeted and Effective Photodynamic Therapy. *Photodiagn. Photodyn. Ther.* **2017**, *19*, 212–220.
- (26) Chen, C. W.; Chan, Y. C.; Hsiao, M.; Liu, R. S. Plasmon-Enhanced Photodynamic Cancer Therapy by Upconversion Nanoparticles Conjugated with Au Nanorods. *ACS Appl. Mater. Interfaces* **2016**, *8*, 32108–32119.
- (27) Monaco, I.; Arena, F.; Biffi, S.; Locatelli, E.; Bortot, B.; La Cava, F.; Marini, G. M.; Severini, G. M.; Terreno, E.; Comes, F. M. Synthesis of Lipophilic Core-Shell Fe<sub>3</sub>O<sub>4</sub>@SiO<sub>2</sub>@Au Nanoparticles and Polymeric Entrapment into Nano-Micelle. A Novel Nanosystem for in Vivo Active Targeting and Magnetic Resonance/ Photoacoustic Dual-Imaging. *Bioconjugate Chem.* **2017**, *28*, 1382–1390.
- (28) Pan, J.; Feng, S.-S. Targeting and Imaging Cancer Cells by Folate-Decorated, Quantum Dots (Qds)-Loaded Nanoparticles of Biodegradable Polymers. *Biomaterials* **2009**, *30*, 1176–1183.
- (29) Di Felice, R.; Selloni, A. Adsorption Modes of Cysteine on Au(111): Thiolate, Amino-Thiolate, Disulfide. *J. Chem. Phys.* **2004**, *120*, 4906–4914.
- (30) Karamipour, Sh.; Sadjadia, M. S.; Farhadyarb, N. Fabrication and Spectroscopic Studies of Folic Acid-Conjugated Fe<sub>3</sub>O<sub>4</sub>@Au Core–Shell for Targeted Drug Delivery Application. *Spectrochim. Acta, Part A* **2015**, *148*, 146–155.
- (31) Que, Y.; Feng, C.; Lu, G.; Huang, X. Polymer-Coated Ultrastable and Biofunctionalizable Lanthanide Nanoparticles. *ACS Appl. Mater. Interfaces* **2017**, *9*, 14647–14655.
- (32) Ma, X.; Zhao, Y.; Ng, K. W.; Zhao, Y. Integrated Hollow Mesoporous Silica Nanoparticles for Target Drug/siRNA Co-Delivery. *Chem. - Eur. J.* **2013**, *19*, 15593–15603.
- (33) Rzayev, Z. M.; Khalilova, S.; Salimi, K. Folic Acid Conjugated and Ag-Carrying Organoclay Nanoparticles and Their Response to L929

Fibroblast and DLD-1 Cancer Cells. *J. Microencapsulation* **2017**, *34*, 10–20.

(34) Cheng, W.; Nie, J.; Xu, L.; Liang, C.; Peng, Y.; Liu, G.; Wang, T.; Mei, L.; Huang, L.; Zeng, X. A pH-Sensitive Delivery Vehicle Based on Folic Acid-Conjugated Polydopamine Modified Mesoporous Silica Nanoparticles for Targeted Cancer Therapy. *ACS Appl. Mater. Interfaces* **2017**, *9*, 18462–18473.

(35) Sukhorukova, I. V.; Zhitnyak, I. Y.; Kovalskii, A. M.; Matveev, A. T.; Lebedev, O. I.; Li, X.; Gloushankova, N. A.; Golberg, D.; Shtansky, D. V. Boron Nitride Nanoparticles with a Petal-Like Surface as Anticancer Drug-Delivery Systems. *ACS Appl. Mater. Interfaces* **2015**, *7*, 17217–17225.

(36) Zhitnyak, I. Y.; Bychkov, I. N.; Sukhorukova, I. V.; Kovalskii, A. M.; Firestein, K. L.; Golberg, D.; Gloushankova, N. A.; Shtansky, D. V. Effect of BN Nanoparticles Loaded with Doxorubicin on Tumor Cells with Multiple Drug Resistance. *ACS Appl. Mater. Interfaces* **2017**, *9*, 32498–32508.

(37) Karamipour, Sh.; Sadjadi, M. S.; Farhadyar, N. Fabrication and Spectroscopic Studies of Folic Acid-Conjugated  $\text{Fe}_3\text{O}_4@\text{Au}$  Core–Shell for Targeted Drug Delivery Application. *Spectrochim. Acta, Part A* **2015**, *148*, 146–155.

(38) Hohenberg, P.; Kohn, W. Inhomogeneous Electron Gas. *Phys. Rev.* **1964**, *136*, 864–871.

(39) Kohn, W.; Sham, L. J. Self-Consistent Equations Including Exchange and Correlation Effects. *Phys. Rev.* **1965**, *140*, 1133–1138.

(40) Troullier, N.; Martins, J. L. Efficient Pseudopotentials for Plane-Wave Calculations. *Phys. Rev. B: Condens. Matter Mater. Phys.* **1991**, *43*, 1993–2006.

(41) Kresse, G.; Hafner, J. Ab Initio Molecular Dynamics for Liquid Metals. *Phys. Rev. B: Condens. Matter Mater. Phys.* **1993**, *47*, 558–561.

(42) Kresse, G.; Hafner, J. Ab Initio Molecular-Dynamics Simulation of the Liquid-Metal-Amorphous-Semiconductor Transition in Germanium. *Phys. Rev. B: Condens. Matter Mater. Phys.* **1994**, *49*, 14251–14269.

(43) Kresse, G.; Furthmüller, J. Efficient Iterative Schemes for Ab Initio Total-Energy Calculations Using a Plane-Wave Basis Set. *Phys. Rev. B: Condens. Matter Mater. Phys.* **1996**, *54*, 11169–11186.

(44) Monkhorst, H. J.; Pack, J. D. Special Points for Brillouin-Zone Integrations. *Phys. Rev.* **1976**, *13*, 5188–5192.

(45) Pease, R. S. Crystal Structure of Boron Nitride. *Nature* **1950**, *165*, 722–723.

(46) Chen, S.; Kimura, K. Synthesis and Characterization of Carboxylate-Modified Gold Nanoparticle Powders Dispersible in Water. *Langmuir* **1999**, *15*, 1075–1082.

(47) Moon, O. M.; Kang, B. C.; Lee, S. B.; Boo, J. H. Temperature Effect on Structural Properties of Boron Oxide Thin Films Deposited by moCVD Method. *Thin Solid Films* **2004**, *464–465*, 164–169.